

RSC Advances



This is an *Accepted Manuscript*, which has been through the Royal Society of Chemistry peer review process and has been accepted for publication.

Accepted Manuscripts are published online shortly after acceptance, before technical editing, formatting and proof reading. Using this free service, authors can make their results available to the community, in citable form, before we publish the edited article. This *Accepted Manuscript* will be replaced by the edited, formatted and paginated article as soon as this is available.

You can find more information about *Accepted Manuscripts* in the [Information for Authors](#).

Please note that technical editing may introduce minor changes to the text and/or graphics, which may alter content. The journal's standard [Terms & Conditions](#) and the [Ethical guidelines](#) still apply. In no event shall the Royal Society of Chemistry be held responsible for any errors or omissions in this *Accepted Manuscript* or any consequences arising from the use of any information it contains.

Effect of film thickness and crystallinity on the thermoelectric properties of doped P3HT films

Cheon Taek Hong,^{ab} Youngjae Yoo,^a Young Hun Kang,^a Juwhan Ryu,^b Song Yun Cho^{*a} and Kwang-Suk Jang^{*a}

^a*Division of Advanced Materials, Korea Research Institute of Chemical Technology, Daejeon 305-600, Republic of Korea. E-mail: kjang@kriict.re.kr; scho@kriict.re.kr*

^b*Department of Polymer Science and Engineering, Chungnam National University, Daejeon 305-764, Republic of Korea*

Abstract

The influence of film thickness and crystallinity of poly(3-hexylthiophene) (P3HT) on the thermoelectric properties of doped P3HT films was systematically investigated. To obtain excellent thermoelectric properties, highly crystalline P3HT films were prepared by simple wire-bar-coating. The P3HT films doped with a ferric chloride exhibited power factors of up to $35.0 \mu\text{W m}^{-1}\text{K}^{-2}$ at room temperature. This study suggests that it could be possible to optimize the thermoelectric properties of the conjugated polymer films by controlling the film thickness and polymer structure. Further, the processing method and conjugated polymers selected for thermoelectric applications should be considered carefully because it determines the final characteristics of the films produced.

Introduction

Thermoelectric materials can transform heat to electrical energy *via* the Seebeck effect. Thus, high-performance thermoelectric materials are presumed to effectively convert waste heat to electricity. Although a variety of high-performance inorganic thermoelectric materials have been developed, their application is limited because of their brittleness and poor processability. Recently considerable attention has been given to polymer-based thermoelectric materials because they are promising materials for creating thermoelectric generators that are flexible, printable, and low-cost.¹⁻¹¹ However, the development of high-performance polymer-based thermoelectric materials and/or low-cost printing processes for more integrated devices is still required because polymers have demonstrated relatively poor thermoelectric performance. As a rule, the generator with the highest performance and/or most densely integrated thermoelectric elements demonstrates the best power output. The performance of thermoelectric materials is evaluated by the dimensionless figure of merit, $ZT = S^2\sigma T/\kappa$, where S is the Seebeck coefficient, σ is the electrical conductivity, T is the absolute temperature, and κ is the thermal conductivity. It is difficult to measure the thermal conductivity of thin films directly, therefore an alternative is to use the power factor ($S^2\sigma$), which is based on the product of the square of the Seebeck coefficient and the electrical conductivity, to evaluate thermoelectric performance.

Among the various conjugated polymers, poly(3,4-ethylenedioxythiophene) (PEDOT) is the most widely used in applications requiring a polymer-based thermoelectric material.⁴⁻⁸ Crispin *et al.* reported that PEDOT films doped with a tosylate anion exhibited a ZT of up to 0.25 at room temperature.⁴ In addition, Pipe *et al.* reported that PEDOT films doped with a poly(styrenesulphonate) exhibited a ZT of up to 0.42 at room temperature.⁵ Further, Kim *et al.* reported that PEDOT films electrochemically prepared with a pyridine, poly(ethylene

glycol)-*block*-poly(propylene glycol)-*block*-poly(ethylene glycol) triblock copolymer, and a ferric tosylate, exhibited power factors of up to $1,270 \mu\text{W m}^{-1}\text{K}^{-2}$ at room temperature.⁶ The optimized performance of the aforementioned doped PEDOT films was obtained by precise chemical or electrochemical control of the oxidation level.

Poly(3-hexylthiophene) (P3HT) has also been considered an attractive thermoelectric material and unlike many other conjugated polymers such as PEDOT, P3HT is soluble in common organic solvents.⁹⁻¹¹ This solubility renders P3HT a suitable thermoelectric polymer for various solution-processes including bar-coating, screen-printing, and inkjet-printing. However, P3HT film doped with a ferric chloride exhibited a power factor of only $1.9 \mu\text{W m}^{-1}\text{K}^{-2}$ at room temperature,⁹ indicating that the thermoelectric performance of P3HT films requires improvement.

To improve the power factor of P3HT films, Zhu *et al.* used ferric salt of triflimide anions as dopants, and the resultant doped P3HT films exhibited power factors of up to $26 \mu\text{W m}^{-1}\text{K}^{-2}$ at a temperature of 300 - 340 K.⁹ P3HT-based thermoelectric composites has also been reported in a study by Qiu *et al.* wherein composite films of Bi_2Te_3 nanowires and P3HT doped with a ferric chloride demonstrated power factors of $13.6 \mu\text{W m}^{-1}\text{K}^{-2}$ at room temperature.¹⁰ Müller *et al.* reported that composite films of carbon nanotubes and P3HT doped with a ferric chloride exhibited power factors of $95 \pm 12 \mu\text{W m}^{-1}\text{K}^{-2}$ at room temperature.¹¹ However, the morphologies and thicknesses of the aforementioned P3HT and P3HT-based composite films were not carefully controlled because the films were primarily prepared by the drop-casting method. Although the effects of film morphology and thickness on the electrical properties of conjugated polymer films has been extensively studied,¹²⁻¹⁹ a direct relationship between these film characteristics and the thermoelectric properties of conjugated polymers has rarely been reported.

In this study, doped P3HT films were prepared by simple wire-bar-coating. Interestingly, the solution concentration markedly affected the molecular chain packing of P3HT and the film thickness. In addition, it was determined that the thermoelectric properties of the doped P3HT films could be optimized by controlling the film thickness and crystallinity of P3HT chains. The doped P3HT films prepared by wire-bar-coating exhibited power factors of up to 35.0 $\mu\text{W m}^{-1}\text{K}^{-2}$ at room temperature.

Experimental section

Regioregular P3HT (M_w 37,685 g mol⁻¹, regioregularity 98.5%), anhydrous ferric chloride, and nitromethane were purchased from Sigma-Aldrich. *o*-Dichlorobenzene (*o*DCB) was purchased from Junsei. All chemicals in this study were used as received.

The P3HT was dissolved in *o*DCB to prepare solutions with concentrations of 10, 20, 30, 50, and 150 mg mL⁻¹, respectively. To provide a smooth substrate layer and prevent detachment of the P3HT film during the doping process, polyimide precursor was spin-coated onto a glass substrate (76 mm × 26 mm) and annealed. Preparation of the polyimide precursor, which is composed of monomers of 3,3',4,4'-biphenyltetracarboxylic dianhydride and *p*-phenylenediamine, and the detailed fabrication procedure of the polyimide thin films are described elsewhere.²⁰ The thickness of the polyimide interlayer was restricted to 60 nm. For the precise bar-coating process, a 1.3 cm diameter bar that was closely wound with a 0.21 mm diameter wire was used and the carrying speed of the wire-bar was maintained at 10 mm/s. Following bar-coating and attachment onto the polyimide-treated substrate, the generated films were dried at room temperature for 2 hr, followed by annealing at 90 °C for 10 min and 150 °C for 30 min, respectively, on a hot plate. The annealed P3HT films were

doped by immersion in 0.03 M FeCl₃/nitromethane solution for 1 hr. The doped P3HT films were finally rinsed with methanol to remove excess dopants, and annealed at 90 °C for 10 min to remove any remaining solvent.

The Seebeck coefficients of the prepared films were measured under dark ambient conditions utilizing a custom system built onsite. Before the measurement, 50 nm-thick gold electrodes were deposited by thermal evaporation onto the P3HT films through a shadow mask. The distance between the two electrodes was 20 mm and the width of each electrode was 5 mm. The temperature gradient between the electrodes was varied from 1 to 15 °C. The thermoelectric voltage generated by the temperature difference was measured with a Keithley 2182A Nanovoltmeter. The electrical conductivity was measured by a four-probe method (Loresta GP Model MCP-T610, Mitsubishi Chemical). The thickness of the P3HT layers was determined with an alpha-step surface profiler (α -step DC50, KLA Tencor). The atomic force microscope (AFM) images were obtained with a tapping mode AFM (Nanoscope IV, Digital Instruments). The X-ray diffraction (XRD) patterns were obtained with a Rigaku D/MAX-2200V diffractometer using a Cu K α radiation source.

Results and discussion

P3HT films were prepared by a simple wire-bar-coating process (Fig. 1). By varying the diameter size of the wire wound closely onto the bar surface, the volume of the gap between the wire-bar and the substrate can be precisely determined. It is established that the wire diameter, carrying speed of the wire-bar, and solid content of the coating solution can significantly affect the film thickness and quality.²¹⁻²³ In this study, to precisely control the film thickness, only the concentration of the coating solution was varied, while all other

parameters such as wire diameter and carrying speed of the wire-bar were kept constant. P3HT/*o*DCB solutions with concentrations of 10, 20, 30, and 50 mg mL⁻¹ were prepared using magnetic stirring, while a mortar and pestle were used to prepare a P3HT/*o*DCB paste with a concentration of 150 mg mL⁻¹. Fig. 2 displays the variation of thickness of P3HT films as a function of the solution concentration. The film thickness ranged varied from 520 nm to 4.1 μm, and became saturated at 50 mg mL⁻¹. The thickness of P3HT films from 50 mg mL⁻¹ and 150 mg mL⁻¹ P3HT/*o*DCB was 4.0 and 4.1 μm, respectively, revealing no considerable difference in film thickness. Fig. 3 displays the AFM images of the as-prepared P3HT films. Interestingly, the nanowire morphology at the film surface is more apparent as the concentration of the coating solution increases. It has been previously reported that P3HT crystallizes in films by forming crystalline nanorods or nanowires that have diameters of 10 - 30 nm and lengths of a hundred nanometers to a few microns.¹⁵⁻¹⁹ The increased crystallinity of P3HT, along with the favorable nanorod/nanowire morphology, is the result of the maximized stacking of the P3HT chains that is induced by the π-π interaction of their macromolecular backbones. The XRD patterns of the as-prepared P3HT films (Fig. 4) were used to determine that all of the patterns observed are the result of the lamellar packing of P3HT. As the concentration and the resulting film thickness increase, intensity of the first-order peak also increases. The peak intensities of the films from P3HT/*o*DCB solution with a concentration of 50 mg mL⁻¹ (Fig. 4d) and those from the paste with a concentration of 150 mg mL⁻¹ (Fig. 4e) could be directly compared because any influence of the difference in film thickness on the XRD intensity is believed to be negligible. The presence of higher intensity peaks in the pattern of the film from the P3HT/*o*DCB paste compared to the peaks in the solution-based film indicates that it has a more highly ordered structure of P3HT chains. Further, this result is in agreement with the AFM image in Fig. 3 that reveals a more discernible nanowire structure in the film from the P3HT/*o*DCB paste than in those from the

P3HT/*o*DCB solutions. The origin of the difference in XRD intensity between the films from P3HT/*o*DCB solution (50 mg mL⁻¹) and paste (150 mg mL⁻¹) is unclear, however it may be related to the increased crystallinity of P3HT in the gel-like paste state. This rationale for this postulation can be derived from a previous study that found that the viscosity and crystallinity of P3HT solutions increase dramatically during shear.²⁴ During mixing with the mortar and pestle utilized in this study, the P3HT/*o*DCB paste may experience sufficient shear force to form P3HT crystals. It can be concluded from the surface morphologies and XRD peak intensities that the concentration of the coating solution could affect the molecular chain packing of P3HT.

The as-prepared P3HT films are not electrically conductive, therefore doping of the P3HT films is required to enable their use in thermoelectric applications. To obtain highly doped P3HT with a high electrical conductivity, the P3HT films were immersed in 0.03 M FeCl₃/nitromethane solution for 1 hr. During the doping process, dopant molecules are incorporated into the P3HT layers. The AFM images of the doped P3HT films reveal the presence of particles with diameters of 25 - 130 nm on the film surface (Fig. 5). There does not appear to be meaningful difference in the surface morphology among the different doped P3HT films, perhaps because of the sizeable morphological change in the P3HT films, induced by dopant insertion during the doping process. It is also presumed that such insertion causes the structural change of P3HT from a nanowire-like structure to a nanoparticle-like structure. To observe diffraction patterns of the doped P3HT films, the films were investigated by XRD as shown in Fig. 6. The XRD peaks are slightly shifted to lower angles compared to those of the as-prepared films because of the dopant insertion during the doping process. In the XRD patterns of the films from P3HT/*o*DCB solutions with lower concentrations such as 10, 20, and 30 mg mL⁻¹, there are two first-order peaks which are

assigned to ($1'00$) and (100) reflections. The existence of the broad ($1'00$) peaks at the lower angle indicates that excessive expansion in the P3HT interchain distance occurred during the dopant insertion. The broad peaks may be the result of the damage incurred by the crystalline structure of P3HT during the doping and washing process, which could more seriously affect thinner crystal films. Alternatively, the XRD patterns of the doped P3HT films from the most highly concentrated solutions (50 and 150 mg mL⁻¹) display no broad peaks within the lower angle region. It is presumed that the damage to the crystalline structure was predominantly present at the collapsed film surface because dopant insertion and removal of excess dopants are initiated from the surface of the P3HT films. Interestingly, the first-order peak intensity of the film from P3HT/*o*DCB paste is much higher than that from the P3HT/*o*DCB solution with a concentration of 50 mg mL⁻¹, irrespectively of the doping process. This result indicates that the concentration of the coating solution and the film thickness apparently affect the molecular chain packing of P3HT even after the doping process.

To estimate the thermoelectric properties of the doped P3HT films as a function of film thickness, the thickness-dependent Seebeck coefficients, electrical conductivities, and power factors were measured, as shown in Fig. 7. The concentration of the coating solutions and the resulting film thickness appreciably affect the thermoelectric properties of the doped P3HT films. As the film thickness increases, the Seebeck coefficient decreases and the electrical conductivity increases. The power factor, calculated from the measured Seebeck coefficient and electrical conductivity, increases as the film thickness increases. The thermoelectric properties of conjugated polymers are directly related to the doping levels.⁴⁻⁸ As a rule, the doping level of conjugated polymers increases, the Seebeck coefficient decreases, and the electrical conductivity increases. This observation implies that the power factor and ZT values of conjugated polymers could potentially be tuned by controlling the doping level. The

relatively poor thermoelectric properties of the doped P3HT films from low-concentration solutions correlated with the doping level and the damage inflicted upon the crystalline structure of the P3HT. The lower thickness of the P3HT films might result in a relatively higher dedoping amount during the washing process. To facilitate the comparison, we prepared a spin-coated P3HT film with a thickness of 200 nm. Following the same doping and washing process, the film was not electrically conductive due to the full dedoping during the washing process. The XRD patterns of the doped P3HT films from low-concentration solutions contain broad ($1'00$) peaks at the lower angle that are indicative of increased expansion of the P3HT chains. It is possible that this expansion is caused by the dedoping and the resulting damage to the crystalline structure of P3HT that occurs during the washing process. The combination of the high level of dedoping and the collapsed crystalline structure induced low electrical conductivity within the polymer film that had a detrimental effect on the observed thermoelectric properties. The doped P3HT films prepared from P3HT/*o*DCB solution and paste with concentrations of 50 and 150 mg mL⁻¹, respectively, exhibited higher thermoelectric properties as compared to those created from lower concentrations of P3HT/*o*DCB solution. Interestingly, although there is a negligible difference in film thickness between the film formed from P3HT/*o*DCB paste and that of the 50 mg mL⁻¹ solution, the paste-based film demonstrated relatively superior thermoelectric properties. The Seebeck coefficient, electrical conductivity, and power factor of the doped P3HT films prepared from 150 mg mL⁻¹ P3HT/*o*DCB paste were 37.2 μ V K⁻¹, 254 S cm⁻¹, and 35.0 μ W m⁻¹K⁻², respectively. The higher electrical conductivity and resulting increase in power factor observed may be related to the molecular chain packing of P3HT, because P3HT films with higher crystallinity are advantageous for charge transport.¹⁵⁻¹⁹ The highly crystalline nature of the P3HT films created from P3HT/*o*DCB paste was confirmed by the XRD study. The effect of P3HT structure, *i.e.* crystallinity and morphology, on device performance of thin-film

transistors and photovoltaics has been previously reported.¹⁵⁻¹⁹ However, the effect of the conjugated polymer structure on the thermoelectric properties of devices is still unknown because of a lack of research in this area. The results of this study indicate that the crystallinity and morphology of polymer-based thermoelectric materials should be considered to maximize their promise for use in thermoelectric applications. By controlling the film thickness and polymer structure, thermoelectric properties of conjugated polymers could be optimized. The research works for investigating the effect of film thickness and crystallinity of other conjugated polymers such as polyaniline and PEDOT are currently being investigated.

Conclusion

In summary, we prepared doped P3HT films by simple wire-bar-coating where in the film thickness was controlled by varying the concentration of the coating solution. As the solution concentration increased, the Seebeck coefficient decreased and the electrical conductivity and the calculated power factor increased. The power factor demonstrated in this study ($35.0 \mu\text{W m}^{-1}\text{K}^{-2}$) is, to the best of our knowledge, one of the highest power factors determined for P3HT films, as summarized in Table 1. It is expected that the thermoelectric properties of the conjugated polymers could be tuned by controlling the film thickness and polymer structure. In this study, doped conjugated polymers with crystalline structures were generated and determined to be very promising candidate materials for room temperature thermoelectric applications.

Acknowledgements

This work was supported by the KRICT Core Project (KK-1407-B6), a grant from the R&D

Convergence Program funded by the National Research Council of Science & Technology, and the Center for Advanced Soft-Electronics funded by the Ministry of Science, ICT and Future Planning as Global Frontier Project (2011-0031628).

Notes and references

- 1 M. He, F. Qiu and Z. Lin, *Energy Environ. Sci.*, 2013, **6**, 1352.
- 2 M. Chanbinyc, *Nat. Mater.*, 2014, **13**, 119.
- 3 Y. Sun, P. Sheng, C. Di, F. Jiao, W. Xu, D. Qiu and D. Zhu, *Adv. Mater.*, 2012, **24**, 932.
- 4 O. Bubnova, Z. U. Khan, A. Malti, S. Braun, M. Fahlman, M. Berggren and X. Cripsin, *Nat. Mater.*, 2011, **10**, 429.
- 5 G-H. Kim, L. Shao, K. Zhang and K. P. pipe, *Nat. Mater.*, 2013, **12**, 719.
- 6 T. Park, C. Park, B. Kim, H. Shin and E. Kim, *Energy Environ. Sci.*, 2013, **6**, 788
- 7 S. H. Lee, H. Park, S. Kim, W. Son, I. W. Cheong and J. H. Kim, *J. Mater. Chem. A*, 2014, **2**, 7288.
- 8 M. Culebras, C. M. Gómez and A. Cantarero, *J. Mater. Chem. A*, 2014, **2**, 10109.
- 9 Q. Zhang, Y. Sun, W. Xu and D. Zhu, *Energy Environ. Sci.*, 2012, **5**, 9639.
- 10 M. He, J. Ge, Z. Lin, X. Feng, X. Wang, H. Lu, Y. Yang and F. Qiu, *Energy Environ. Sci.*, 2012, **5**, 8351.
- 11 C. Bounioux, P. Díaz-Chao, M. Campoy-Quiles, M. S. Martín-González, A. R. Goñi, R. Yerushalmi-Rozen and C. Müller, *Energy Environ. Sci.*, 2013, **6**, 918.
- 12 B. Gburek and V. Wagner, *Org. Electron.*, 2010, **11**, 814.
- 13 L. Reséndiz, M. Estrada, A. Cerdeira, B. Iñiguez and M. J. Deen, *Org. Electron.*, 2010, **11**, 1920.
- 14 H. Yang, E. Glynos, B. Huang and P. F. Green, *J. Phys. Chem. C*, 2013, **117**, 9590.

- 15 X. Yang, J. Loos, S. C. Veenstra, W. J. H. Verhees, M. M. Wienk, J. M. Kroon, M. A. J. Michels and R. A. J. Janssen, *Nano Lett.*, 2005, **5**, 579.
- 16 X. Yang and J. Loos, *Macromolecules*, 2007, **40**, 1353.
- 17 T. Emrick and E. Pentzer, *NPG Asia Mater.*, 2013, **5**, e43.
- 18 J. S. Kim, J. H. Lee, J. H. Park, C. Shim, M. Sim and K. Cho, *Adv. Funct. Mater.*, 2011, **21**, 480.
- 19 Y. D. Park, S. G. Lee, H. S. Lee, D. Kwak, D. H. Lee and K. Cho, *J. Mater. Chem.*, 2011, **21**, 2338.
- 20 T. Ahn, Y. Choi, H. M. Jung and M. Yi, *Org. Electron.*, 2009, **10**, 12.
- 21 J. Ouyang, T.-F. Guo, Y. Yang, H. Higuchi, M. Yoshioka and T. Nagatsuka, *Adv. Mater.*, 2002, **14**, 915.
- 22 D. Khim, H. Han, K.-J. Baeg, J. Kim, S.-W. Kwak, D.-Y. Kim and Y.-Y. Noh, *Adv. Mater.*, 2013, **25**, 4302.
- 23 *Coatings Technology Handbook*, ed. A. A. Tracton, CRC Press, Boca Raton, 2006
- 24 J. J. Wie, N. A. Nguyen, C. D. Cwalina, J. Liu, D. C. Martin and M. E. Mackay, *Macromolecules*, 2014, **47**, 3343.
- 25 X. Xuan, X. Liu, S. Desbief, P. Leclère, M. Fahlman, R. Lazzaroni, M. Berggren, J. Cornil, D. Emin and X. Cripsin, *Phys. Rev. B*, 2010, **82**, 115454.

Figures and table

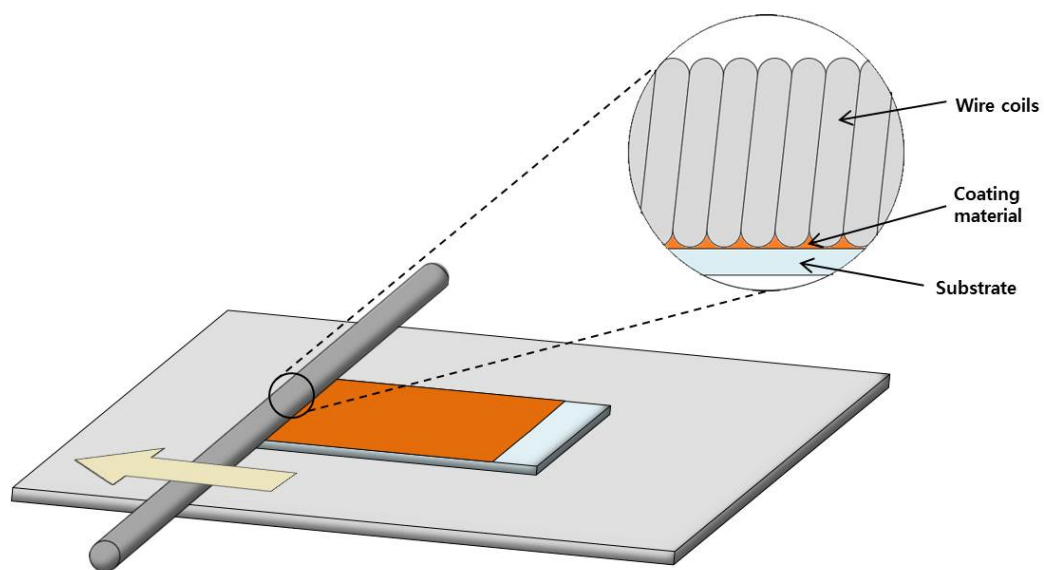


Fig. 1 Schematic diagram of the wire-bar-coating process.

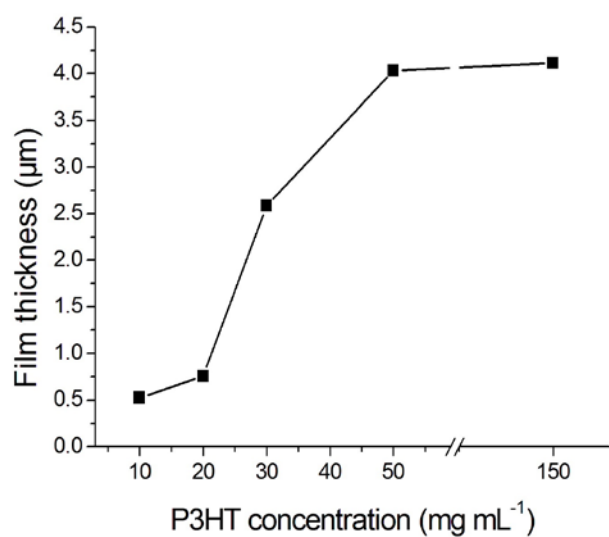


Fig. 2 The variation of P3HT film thickness as a function of the solution concentration.

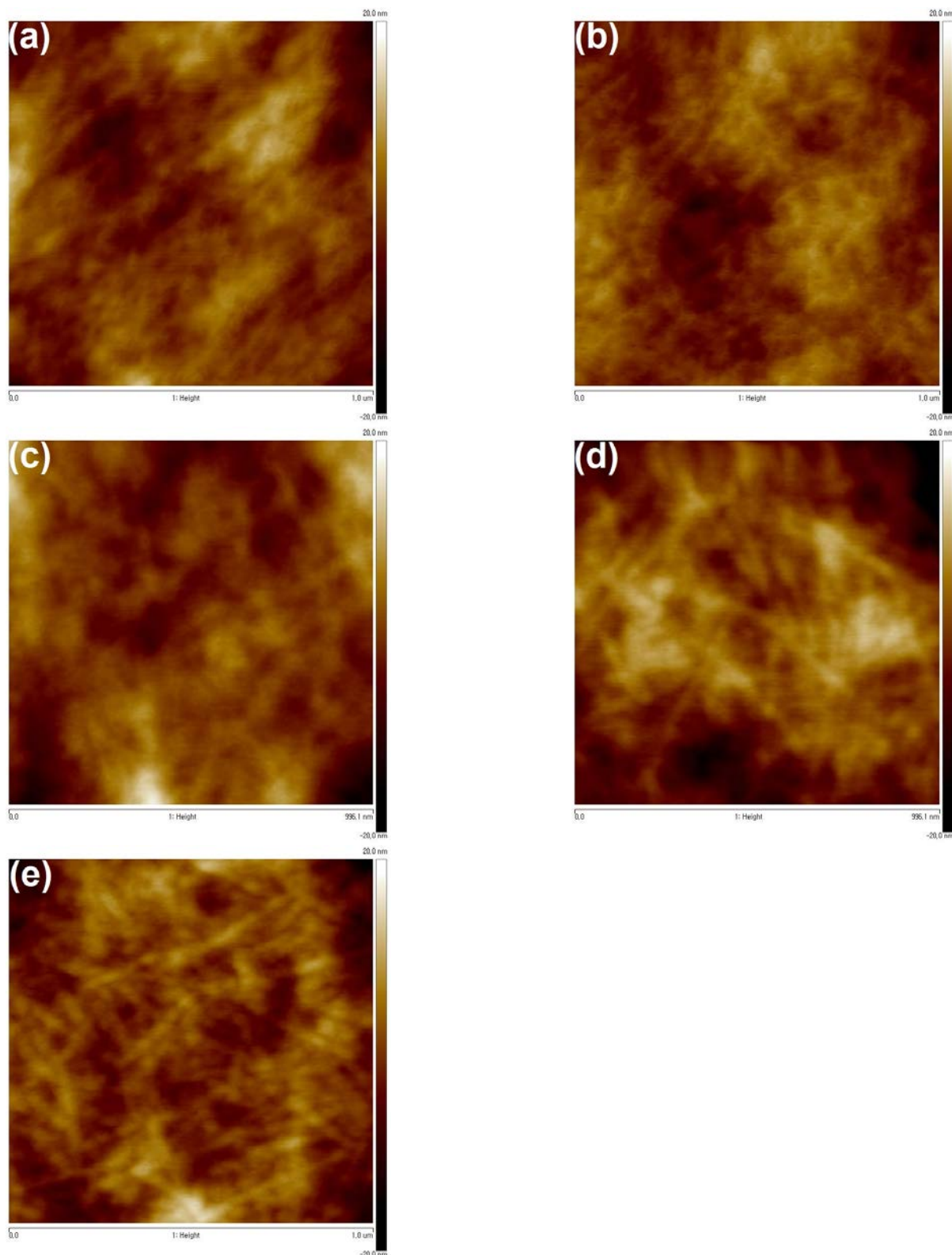


Fig. 3 The AFM images ($1 \mu\text{m} \times 1 \mu\text{m}$) of the as-prepared P3HT films from P3HT/*o*DCB solutions and paste with concentrations of (a) 10, (b) 20, (c) 30, (d) 50, and (e) 150 mg mL^{-1} , respectively.

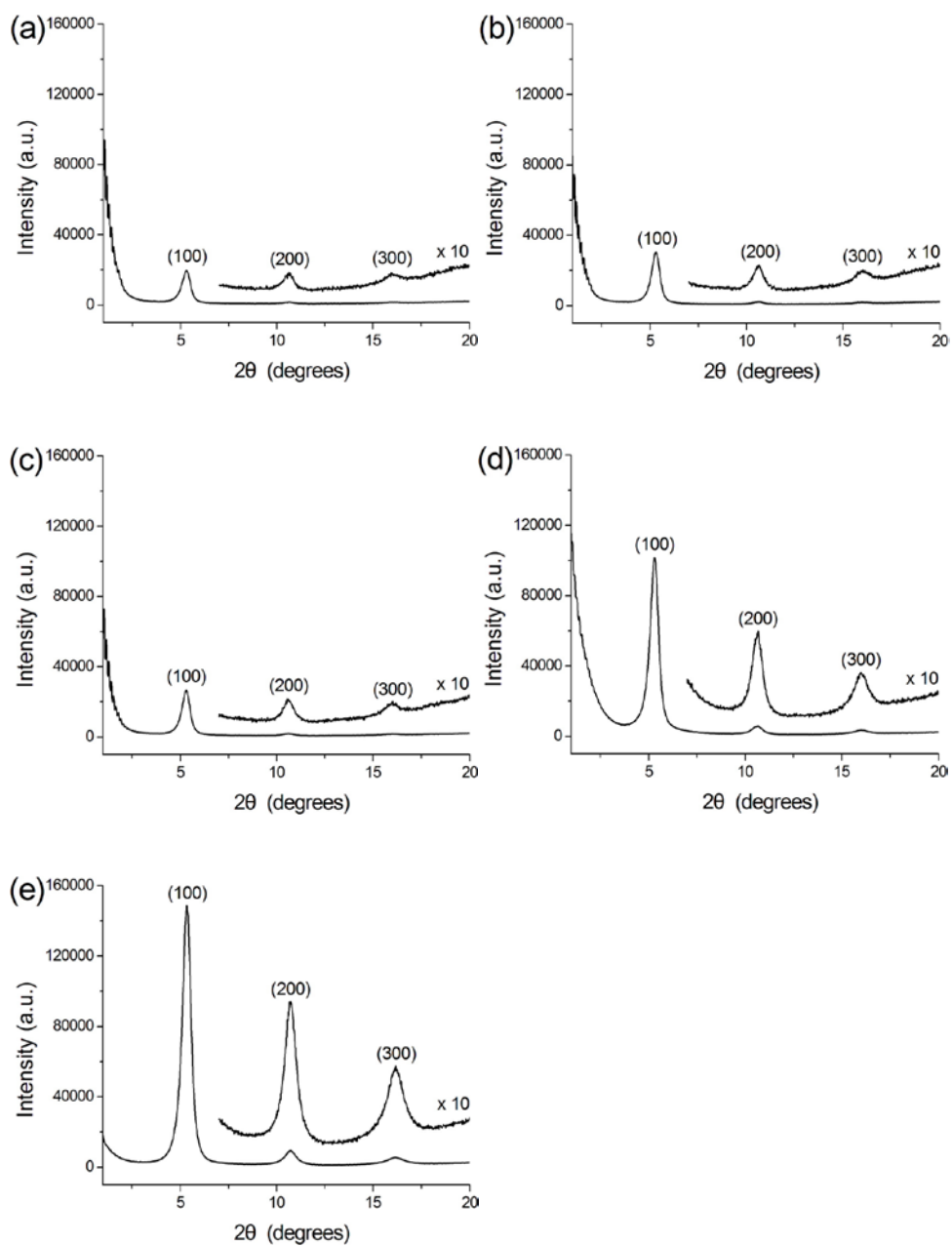


Fig. 4 The XRD patterns of the as-prepared P3HT films from P3HT/*o*DCB solutions and paste with concentrations of (a) 10, (b) 20, (c) 30, (d) 50, and (e) 150 mg mL⁻¹, respectively.

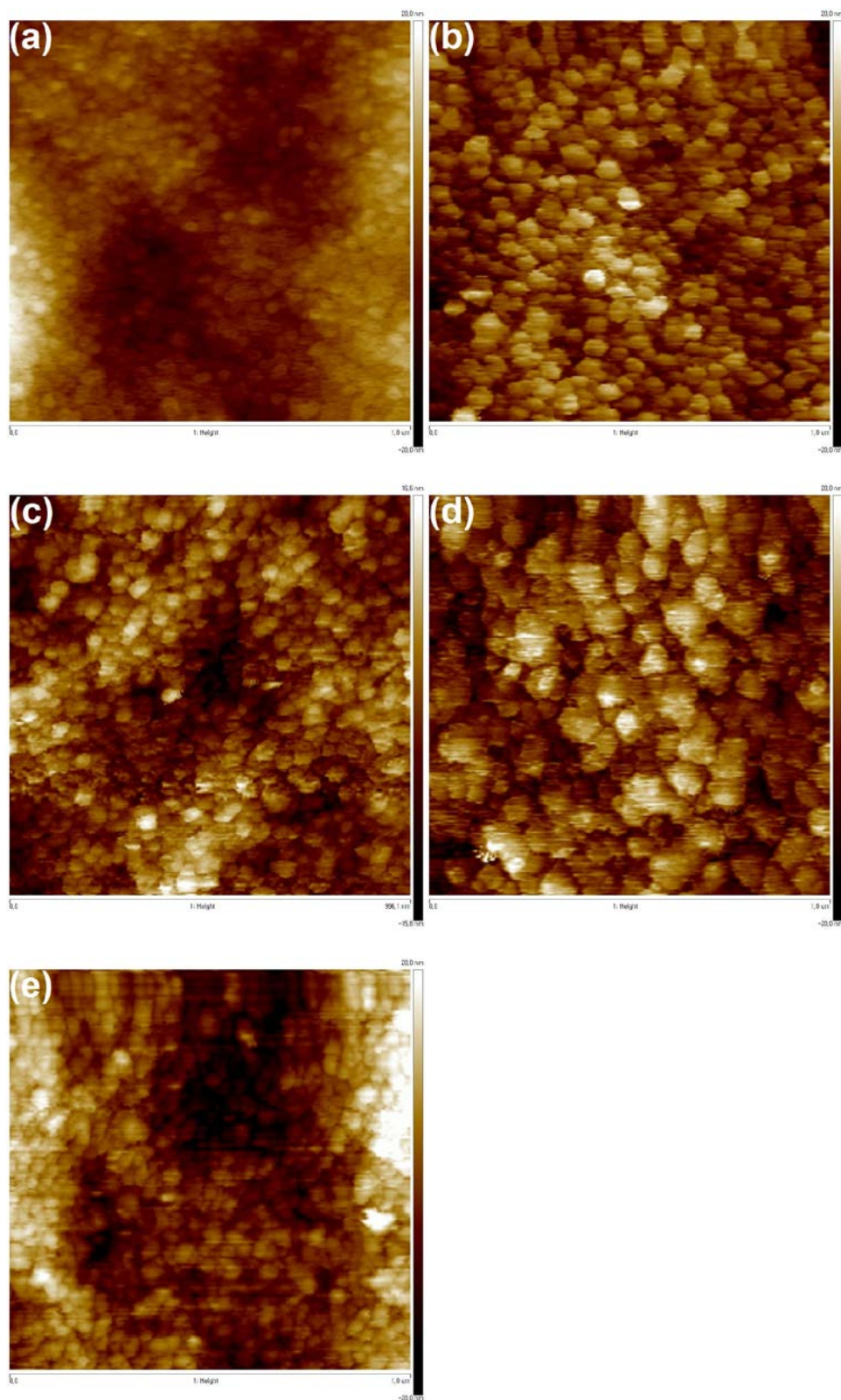


Fig. 5 The AFM images ($1 \mu\text{m} \times 1 \mu\text{m}$) of the doped P3HT films from P3HT/*o*DCB solutions and paste with concentrations of (a) 10, (b) 20, (c) 30, (d) 50, and (e) 150 mg mL^{-1} , respectively.

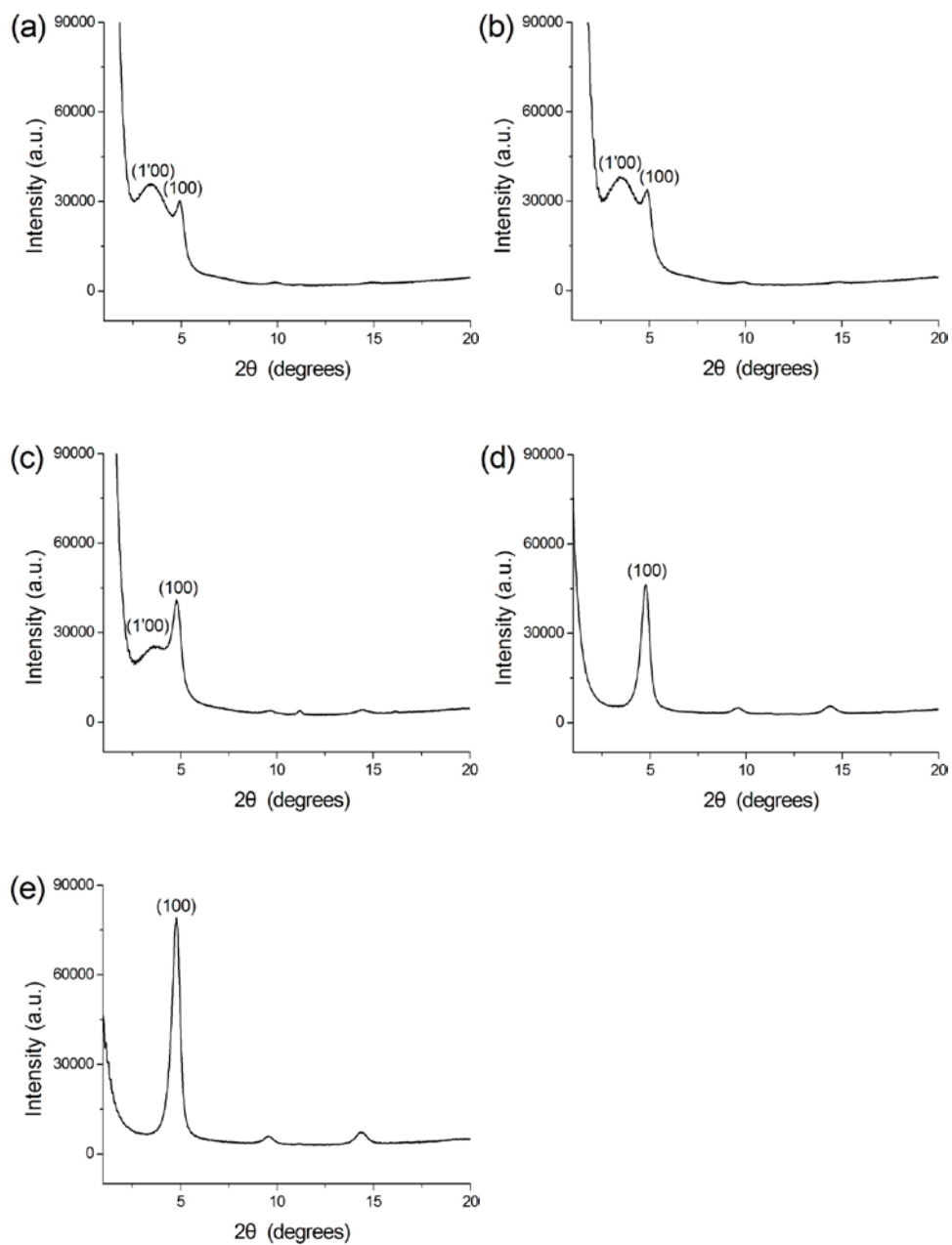


Fig. 6 The XRD patterns of the doped P3HT films from P3HT/*o*DCB solutions and paste with concentrations of (a) 10, (b) 20, (c) 30, (d) 50, and (e) 150 mg mL⁻¹, respectively.

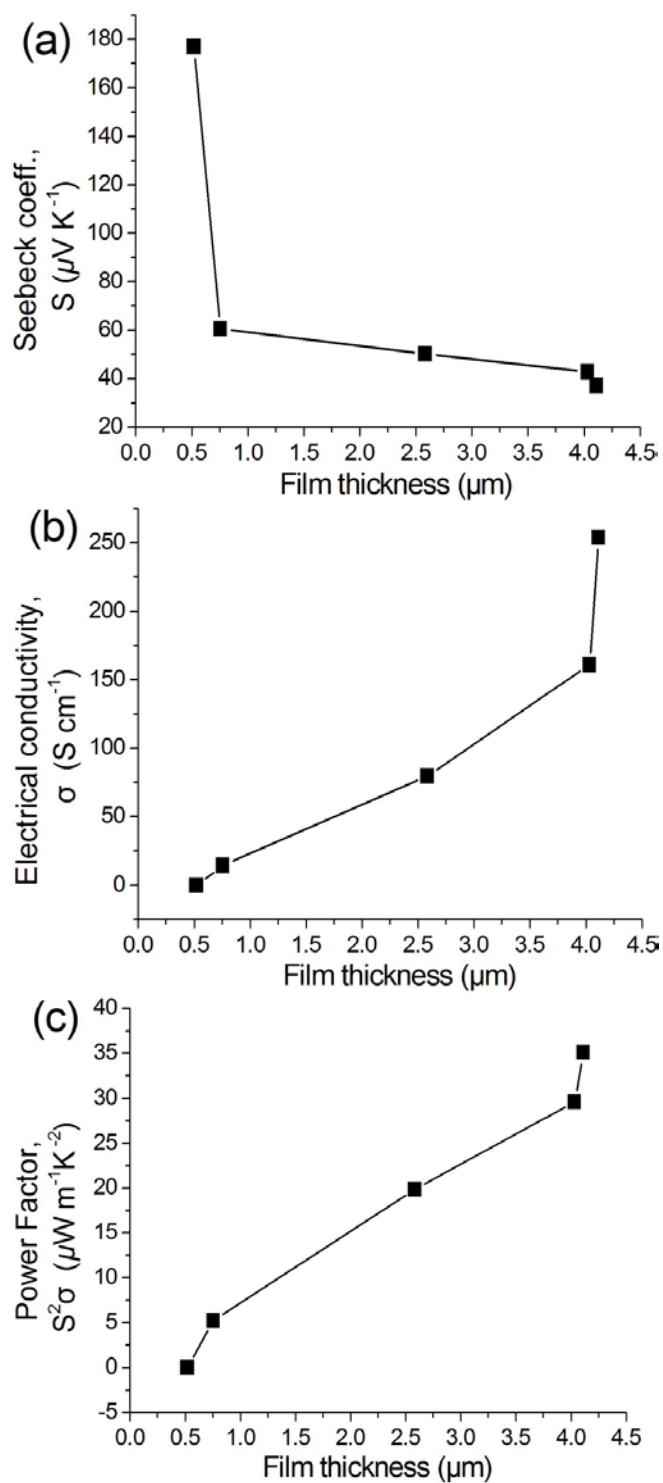


Fig. 7 The thickness dependence of (a) Seebeck coefficients, (b) electrical conductivities, and (c) power factors of the doped P3HT films.

Table 1 Summary of thermoelectric properties of the solution-processed P3HT films, previously reported and measured in this work

Coating method	Dopant	Seebeck coefficient [$\mu\text{V K}^{-1}$]	Electrical conductivity [S cm^{-1}]	Power factor [$\mu\text{W m}^{-1}\text{K}^{-2}$]	Reference #
Drop-casting	FeCl_3	30	21	1.9	[9]
Drop-casting	$(\text{CF}_3\text{SO}_2)_2\text{N}^-$	-	-	26	[9]
Drop-casting	FeCl_3	74	7	3.9	[10]
Drop-casting	NOPF_6	25	2.2	0.14	[25]
Wire-bar-coating	FeCl_3	37.2	254	35.0	This work

Influence of film thickness and crystallinity of poly(3-hexylthiophene) (P3HT) on the thermoelectric properties of doped P3HT films was systematically investigated.

